A COMPARISON BETWEEN THE REVERSE-FLOW OPERATED PACKED BED AND STEADY STATE MONOLITH BED REACTORS FOR CATALYTIC COMBUSTION OF METHANE IN LEAN MIXTURES

Magdalena BOŞOMOIU[1], Grigore BOZGA[2]

Scopul acestei lucrări îl constituie studiul comparativ al performanţelor a două tipuri de reactoare pentru combustia catalitică a metanului, un reactor cu strat granular fix, operat în regim nestaţionar, cu schimbarea periodică a circulaţiei fazei gazoase şi respectiv un reactor cu strat monolitic operat staţionar. Drept catalizator s-a considerat un oxid perovskitic, având o bună activitate în combustia metanului, evidenţiată în studii anterioare. Rezultatele subliniază avantajele operării cu schimbare periodică a sensului de circulaţie a gazului, ca o tehnică simplă de recuperare a căldurii de reacţie şi adecvanţa acesteia la reactoare ce includ capacităţi termice ridicate. De asemenea, sunt evidenţiate caracteristicile straturilor monolitice: cădere mică de presiune a gazului, o bună eficacitate în utilizarea catalizatorului, însă o capacitate calorică mică. Pe de altă parte, straturile granulare, caracterizate de capacităţi calorice mai ridicate, pot asigura o eficienţă ridicată a utilizării catalizatorului, numai la dimensiuni mici ale granulelor, dimensiuni care favorizează creşterea căderii de presiune. Combinând aceste particularităţi, o structură raţională de reactor de combustie apare a fi constituită din trei straturi, din care două granulare, cu dimensiuni relativ ridicate ale granulelor (pentru a limita căderea de presiune) şi respectiv un strat monolitic de catalizator, în poziţie centrală.

The aim of this study is to investigate comparatively the performances of two reactors for the catalytic combustion of lean methane –air mixtures, an unsteady-state packed bed reactor operated with periodic flow reversal and a steady – state monolith bed reactor. As catalyst, in both reactors was considered a perovskite oxide, which proved a good activity for methane combustion in our previous studies. The results are evidencing the advantages of the reverse flow operation, as a simple technique for heat recovery and its suitability for reactors including high thermal capacity beds. Due to the lower pressure drop and good catalyst use effectiveness, the monolith structures present better performances comparing to the packed beds of catalyst, but are characterized by a lower thermal capacity. On the other hand, the packed beds, having the advantage of a higher thermal capacity can insure a convenient effectiveness in the use of catalyst, only at small grain sizes, which are inducing higher pressure drop in the bed. By combining these features a rational structure for an auto-thermal combustion reactor appears to include three beds, of

[1] Drd., Depart. of Chemical Engineering, University POLITEHNICA of Bucharest, Romania
[2] Prof., Depart. of Chemical Engineering, University POLITEHNICA of Bucharest, Romania

which two lateral packed beds of coarse inert particles and a central monolith bed containing the catalyst.

Keywords: reverse-flow reactor, monolith reactor, simulation, catalytic combustion, methane

1. Introduction

The packed bed reactor operated with periodical flow reversal and the monolith bed reactor, are two types of reactors currently used in catalytic combustion for production of energy or depollution of gases. Packed bed reactors with periodic reversal of gas flow are extensively used in catalytic combustion of VOC (volatile organic compounds) due to the advantage of autothermal operation, even at low reagent concentrations (low adiabatic temperature rise of the reaction mixture). This type of reactor was proposed for the catalytic purification of exhaust gases, for the first time, by Boreskov, Matros and Lakhmostov in 1982 (referred by [1]). The principle of this technique consists in the periodical change of the gas flow direction through the catalyst bed, in order to insure the autothermal operation. This is accomplished by the heat transfer from solid to gas, in order to preheat it, at one end of the bed and the store of the heat released in reaction by the solid at the other end.

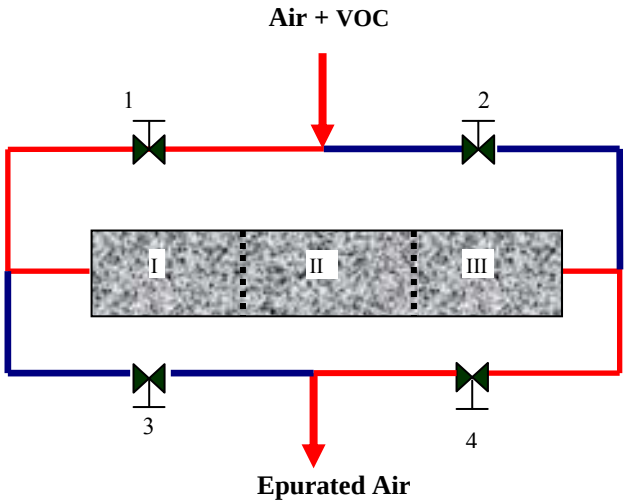

Fig. 1. Connections scheme in packed bed operated with periodical flow reversal

A typical scheme of the packed bed connections, operated in reverse flow unsteady state regime is presented in Fig. 1. When the valves 1 and 4 are open, respectively 2 and 3 are closed, the gas flows from the left to the right (direct flow) and conversely, closing the valves 1 and 4 and opening 2 and 3 the gas is

flowing from the right to the left (reverse flow). Starting the operation with the bed heated at a sufficiently high temperature, T_{S0}, for an exothermic reaction the reactor can be operated autothermally feeding the gas at ambient temperature. Further details concerning the construction and operation principles of a reverse flow reactor are published by Matros and Noskov [1] and Matros [2], where are also evidenced its following advantages [1, 2]:

- a more effective utilization of heat released in the exothermic combustion reactions, by the autothermal reactor operation; practically all this heat is stored in the solid bed, being used for preheating of inlet gases;
- heat exchange occurs directly inside the catalyst bed which, besides its main function of promoting the chemical transformation, plays the role of heat regenerator; thus, it is possible to exclude the recuperative heat exchanger or any other energy supply to preheat the inlet gas mixture up to appropriate temperatures demanded by the total combustion;
- a good stability to fluctuations in feed concentration, temperature and flow rate, due to the considerable ratio between the thermal capacity of the reactor and the heat removed out from the bed by the flowing gas;
- catalytic combustion of low heat value gases in the regime of periodic flow reversal allows to remove the released reaction heat from the hottest areas of the bed, diminishing the peaks of temperature.

A second type of catalytic reactor frequently used in combustion applications is the monolith reactor. The extensive use of monolithic catalyst beds in heterogeneous catalysis has started to be explored only at the beginning of the 1980's decade, after their successful commercial application to the control of automotive exhausts and to the reduction of nitrogen oxides.

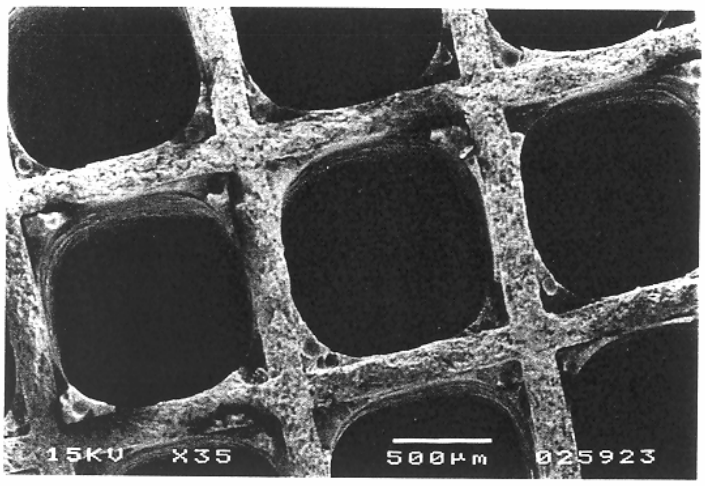

Fig. 2. Scanning electron micrograph of a ceramic monolith with square shaped cells, coated with γ-Al_2O_3 and a suited catalyst for combustion applications [3]

The monolith reactor consists of a honeycomb structure with a large number of parallel channels (having different cross-sectional shapes: circle, triangle, square, hexagonal or sinusoidal) through which gas flows (Fig. 2).

Among the reactors usable for catalytic combustion processes, monolithic reactors have several recognized advantages: lower pressure drop (due to a larger open frontal area), good mechanical strength (required for the conditions encountered in environmental applications) and a potentially smaller size of the reactor in gas-phase processes. A great number of articles, reviews and monographs concerning monolith based reactors and their applications have been published in the last decades [4-8].

Conventional parallel channel monoliths are virtually adiabatic, this being compatible with the processes for the abatement of pollutants in diluted streams (but would severely limit the control of temperature in strong endothermic and exothermic chemical processes [9]).

The VOC combustion catalytic activity for several perovskite catalysts was investigated comparatively with a commercial Pt/alumina catalyst in one of our previous studies [10]. This evidenced a good catalytic activity of the perovskite $La_{0.9}Ce_{0.1}CoO_3$ in the combustion of methane (a reference organic compound in combustion studies). In this work we studied comparatively the performances of the unsteady- state reverse flow and steady- state monolithic reactors based on this catalyst, for the process of methane combustion.

2. Mathematical model

The equations describing the two reactors have essentially the same form, the only difference being the heat and mass accumulation terms present in the unsteady-state models. The adiabatic thermal regimes were considered for both reactors, at operating temperatures permitting to neglect the contribution of the homogeneous reactions to the combustion process, (significant only above 700^{o}C [11]). The mathematical models used in the simulations are given in Table 1. Physical properties of gas, such as density, viscosity and molecular diffusion coefficients are estimated as temperature functions using correlations taken from literature [12].

The combustion kinetics of the lean methane mixtures on the considered perovskite catalyst is described by a first order kinetics in respect with methane [10]:

$$v_{RA} = k_m \, p_{AS}; \quad k_m = 82.15 \, \exp\left(-\frac{9971}{T_S}\right) \text{ kmol/(kg} \cdot \text{s} \cdot \text{bar)} \qquad (1)$$

p_{AS} – partial pressure of methane in catalyst pores.

The mathematical modelling principles of reverse flow reactors are largely described by Matros and Bunimovich [13]. In this study we used a heterogeneous

unsteady-state one - dimensional axial dispersion model, which neglects the heat transferred from the catalyst bed to the wall and then axially back to the inert bed. The considered reactor has the catalyst bed placed between two identical zones of inert grains, having the role to store the heat generated in the combustion process.

Mathematical models of monolith reactors are reviewed by Cybulski and Moulijn [6,7]. For modelling purposes, we considered a honeycomb type structure with square channels, consisting in a solid support on which a thin layer of porous catalytic material (washcoat layer) has been applied.

Table 1.

Mathematical models of the two reactors

RFR

Methane balance in the gas phase:

$$\varepsilon\frac{\partial Y_{AG}}{\partial t}=\varepsilon D_L\frac{\partial^2 Y_{AG}}{\partial z^2}-u\frac{\partial Y_{AG}}{\partial z}-k_G a_v(Y_{AG}-Y_{AS}) \quad (2)$$

Methane balance in the porous catalyst phase:

$$k_G a_v C(Y_{AG}-Y_{AS})=\eta_i\,\rho_S(1-\varepsilon)\,v_{RA} \quad (3)$$

Heat balance for the gas phase:

$$\varepsilon\rho_G\,c_{p,G}\frac{\partial T_G}{\partial t}=\varepsilon\lambda_{L,S}\frac{\partial^2 T_G}{\partial z^2}-u\rho_G\,c_{p,G}\frac{\partial T_G}{\partial z}+\alpha a_v(T_S-T_G) \quad (4)$$

Heat balance for the solid phase:

$$\rho_S(1-\varepsilon)c_{p,S}\frac{\partial T_S}{\partial t}=(1-\varepsilon)\lambda_S\frac{\partial^2 T_S}{\partial z^2}+(-\Delta H_{RA})\,\eta_i\rho_S(1-\varepsilon)v_{RA}-\alpha a_v(T_S-T_G) \quad (5)$$

$$x=0,\ s>0,\ u\cdot(Y_{A0}-Y_{AG})=-\varepsilon D_L\frac{\partial Y_{AG}}{\partial z};\ \rho_G\cdot u\cdot c_{p,G}(T_0-T_G)=-\varepsilon\,\lambda_{L,S}\frac{\partial T_G}{\partial z};\ \frac{\partial T_S}{\partial z}=0$$

(6 -8)

$$x=1,\ s>0 \qquad \frac{\partial Y_{AG}}{\partial z}=\frac{\partial T_G}{\partial z}=\frac{\partial T_S}{\partial z}=0 \quad (9)$$

$$t=0,\ 0\le z\le L,\ Y_{AG}=Y_{Ai}(z);\ T_G=T_{Gi}(z);\ T_S=T_{Si}(z) \quad (10\text{-}12)$$

Monolith reactor

Methane balance in the gas phase:

$$\frac{dY_{AG}}{dz}=\frac{1}{u}\frac{4}{d_h}k_G(Y_{AS}-Y_{AG})\ ;\ z=0\quad Y_{AG}=Y_{A0} \quad (13)$$

Methane balance in the porous catalyst phase:

$$k_G C\,(Y_{AG}-Y_{AS})=\eta_i\,\rho_S L_C v_{RA} \quad (14)$$

Heat balance for the gas phase:

$$\frac{dT_G}{dz}=\frac{1}{u\rho_G\,c_{p,G}}\frac{4}{d_h}\alpha(T_S-T_G)\ ;\ z=0\ \ T_G=T_{G0} \quad (15)$$

Heat balance for the solid phase:

$$\lambda_S\delta_w\frac{d^2T_S}{dz^2}-\alpha(T_S-T_G)+\eta_i(-\Delta H_{RA})\rho_S L_C v_{RA}=0\ ;\ z=0\ \text{şi}\ z=L,\ \frac{dT_S}{dz}=0 \quad (16)$$

All channels of the monolith bed were assumed to have identical behaviour, the velocity distribution uniform among the channels, the catalyst uniformly distributed in the channels and no radial heat loss. For this simulation study, we considered a steady–state one-dimensional heterogeneous plug-flow model for the monolith reactor, accounting for heat conduction in the solid phase (Table 1).

The values of the gas-solid mass and heat transfer coefficients were calculated by the relations given in Table 2. In the same table are presented the relations used in the calculation of the internal effectiveness factors for the two reactors.

Table 2.

Correlations used for different parameters estimation

RFR

Mass and heat gas-solid transfer coefficients:

$Sh = 2 + 1.1 \cdot Sc^{1/3} Re_p^{0,6}$; $3 < Re_p < 10\,000$; $Re_p = u \cdot \rho_G \cdot d_p / \mu_G$ Wakao and Funazkri [14] (17)

$$Nu = 2 + F \cdot Pr^{1/3} \cdot Re_m^{1/2}; \quad F = 0.664 \sqrt{1 + \left[\frac{0.0557\, Re_m^{0.3}\, Pr^{0.67}}{1 + 2.44\left(Pr^{2/3} - 1\right) Re_m^{-0.1}} \right]^2}; \quad Re_m = \frac{Re_p}{\varepsilon}; \tag{18}$$

$100 \le Re_p \le 10\,000$; $Pr \ge 0.6$; Schlünder [15] and Martin [16]

Mass and heat axial dispersion coefficients:

$$\frac{\varepsilon \cdot D_L}{D_A} = 20 + 0.5 \cdot Re_p \cdot Sc \ ; \ Re_p > 5; \ \text{Wakao and Kaguei [17]} \tag{19}$$

$$\frac{1}{Pe_{h,L}} = \frac{1}{Re_p \cdot Pr} \frac{\lambda_{LS}^0}{\lambda_G} + \frac{14.5}{1000 \cdot d_p \left(1 + \frac{0.5}{Re_p \cdot Pr}\right)}; \quad \text{Votruba et al. [18]} \tag{20}$$

$$\frac{\lambda_{LS}^0}{\lambda_G} = \left(\frac{\lambda_S}{\lambda_G}\right)^a ; \ a = 0{,}28 - 0{,}757 \cdot \lg \varepsilon - 0{,}057 \cdot \lg\left(\frac{\lambda_S}{\lambda_G}\right); \ Pe_{h,L} = \frac{u \cdot \rho_G \cdot c_{p,G} \cdot d_p}{\lambda_{L,S}}$$

Internal effectiveness factor:

$$\eta_i = \frac{1}{\varphi_m}\left(\frac{1}{\mathrm{tgh}(3 \cdot \varphi_m)} - \frac{1}{3 \cdot \varphi_m}\right); \ \varphi_m = \frac{d_p}{6}\sqrt{\frac{k_v}{D_e}} \tag{21}$$

$$D_e = \frac{\varepsilon_g}{\tau} \cdot \overline{D}_A \ ; \ \frac{1}{\overline{D}_A} = \frac{1}{D_A} + \frac{1}{D_{K,A}}; \ D_{K,A} = \frac{4}{3} \cdot \overline{r}_p \cdot \left(\frac{2}{\pi} \cdot \frac{R \cdot T_G}{M_A}\right)^{0.5}$$; Froment and Bischoff [19]

$\overline{r}_p$ represents mean pore radius, $1{,}24 \cdot 10^{-7}$m ; $\tau = 4$; $M_A = 16$ kg/kmol

Monolith reactor

Mass and heat gas-solid transfer coefficients:

$$Sh = 2.977\left(1 + 0.095\, Re\, Sc \frac{d_h}{L}\right)^{0.45} \ ; \ k_G = Sh \cdot D_A / d_h \ ; \quad \text{Cybulski and Moulijn [6]} \tag{22}$$

$$Nu = 2.977\left(1 + 0.095\, Re\, Pr \frac{d_h}{L}\right)^{0.45} \ ; \ \alpha = Nu \cdot \lambda_G / d_h \ ; \quad \text{Cybulski and Moulijn [6]} \tag{23}$$

Internal effectiveness factor:

$$\eta_i = \left[1+\left(\frac{1.082}{\varphi^{0.9794}}\right)^{-1.307}\right]^{-\frac{1}{1.307}} \quad ; \quad \varphi = \sqrt{\frac{L_C k_s}{D_e}} \quad ; \quad \text{Leung et al. [20]} \tag{24}$$

3. Results

In order to compare the two reactors for the same productivity, both were considered to be operated at the same weight space velocity, WSV = 1/900 $Nm^3 \cdot kg_{cat}^{-1} \cdot s^{-1}$, the other operating conditions being selected in order to achieve at least 99 % conversion of methane. The fixed bed is packed with spherical porous pellets of the same material as the washcoat, designed to exhibit the same external surface area per unit of reactor volume, as the monolith one. Table 3 summarizes the main features for both reactors. By denoting $\tau = L/u_i$ the space time calculated from the interstitial velocity value at the reactor inlet, one can write:

$$\frac{\varepsilon_1}{\tau_1 \rho_S (1-\varepsilon_1)} = \frac{\varepsilon_2}{\tau_2 \rho_S \varepsilon_{cat\,2}} = \frac{1}{900}\frac{m^3}{kg \cdot s} \tag{25}$$

where indices 1 refers to RFR and 2 to monolith reactor.
From Eq. (18) one obtains $\tau_1 = 0.23$ s and $\tau_2 = 2.03$ m/s. The corresponding values of gas velocity are $u_{i1} = 0.873$ m/s (or $u_1 = 0.35$ m/s) for RFR and $u_{i2} = 0.5$ m/s (or $u_2 = 0.32$ m/s) for the monolith reactor.
A first comparison will concern the pressure drop in the two reactors. In this aim we evaluated mean values of the pressure gradients in the two beds.
For RFR we used Ergun equation [19]:

$$-\frac{dp}{dz} = f_1 \frac{\rho_G \cdot u_1^2}{d_p}, \qquad f_1 = \frac{1-\varepsilon_1}{\varepsilon_1^3}\left(1.75 + 150\frac{1-\varepsilon_1}{Re_p}\right), \; Re_p = \frac{u_1 \rho_G d_p}{\mu_G} \tag{26}$$

For averaged operating conditions in the bed one obtains:

$$-\frac{dp}{dz} = 8.71 \cdot 10^3 \;\; Pa/m$$

For the monolith reactor we calculated the pressure drop according to the correlation proposed by Villermaux and Schweich [21]:

$$-\frac{dp}{dz} = \frac{f_2}{2}\frac{\rho_G \cdot u_{2i}^2}{d_h}, \qquad f_2 = \frac{57}{Re}, \quad Re = \frac{u_{2i} \rho_G d_h}{\mu_G} \tag{27}$$

The pressure drop evaluated at mean gas temperature gives:

$$-\frac{dp}{dz} = 1.13 \cdot 10^3 \;\; Pa/m$$

The results show that the pressure drop for the monolith is approximately one order of magnitude smaller than for the RFR, this representing an important advantage for the cost of operation. However, the values of the two pressure gradients are sufficiently small to be neglected in the calculations of conversion and temperature profiles along the two beds.

Table 3.

Parameter values for the reactors simulation

RFR	
ε_1	0.4 m^3_{gas}/m^3_{bed}
catalyst length	0.2 m
total inert length	0.4 m
d_p	~ 1 mm
T_{G0}	20°C
T_{S0}	400 °C
t_{sc}	360 s
$c_{p,S}$	1100 J/(kg·K)
k_G	0.434 m/s
Monolith reactor	
ε_2	0.66 $m^3_{gas}/m^3_{channel}$
ε_{cat2}	0.112 $m^3_{washcoat}/m^3_{channel}$
L	0.4 m
T_{G0}	520°C
$c_{p,S}$	1128 J/(kg·K)
k_G	0.324 m/s
Common constant parameters	
Y_{A0}	0.001
gas pressure	1 bar
ρ_S	2620 $kg/m^3_{particle}$
a_v	4040 m^2/m^3

For other comparison purposes, simulation studies of the two reactors were performed based on the mathematical models presented in Tables 1 and 2 and the data given in Table 3. The numerical solution of the RFR model is based on the method of orthogonal collocation on finite elements as described by Finlayson [22]. According to this we divided the reactor axis into 7 elements: one element (with eight collocation points) for each inert bed and 5 collocation elements for the catalytic bed (considering 4 collocation points for the elements situated at each end of the catalytic bed and 5 collocation points for the middle elements). The mathematical model of the monolith reactor was solved by applying a discretization method to the heat balance equation of the solid, coupled with an iterative procedure to calculate the solid temperature profile.

An important parameter in the reverse flow operation of a packed bed is the duration of a semi-cycle (or semi-period), t_{sc}, defined as the time elapsed between two consecutive changes of gas flow direction. The duration of an

operation cycle is the double of the semi-cycle, $t_c = 2\ t_{sc}$, being defined as the duration between two consecutive changes in the same direction, of gas flow.

After the start-up of operation is following a transition time during which the temperature and the concentration evolutions along the bed, for the two flow directions become, more and more symmetrical. When the profiles become practically symmetrical, the regime of operation is a pseudo-steady state one. Generally, a relatively high number of flow reversal cycles are necessary (about one hundred) in order to approach the pseudo steady regime of operation. Several temperature and methane conversion evolutions along the bed are presented in Fig. 3 to 6. The number marked on each diagram is representing the cycle or period number, since the beginning of operation.

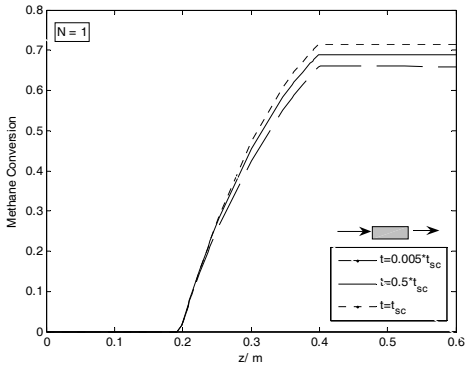

Fig.3. Evolution of methane conversion at different moments of time in the RFR, during the first semi- period (u_0=0.35 m/s;Y_{A0}=0.001;T_{S0}=400°C, t_{sc}=360 s)

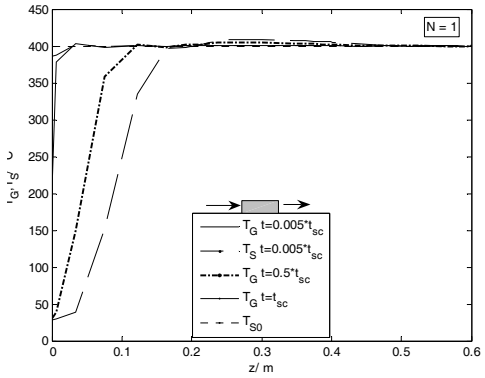

Fig.4. Evolutions of gas phase and solid phase temperatures in the RFR at different moments of time, during the first semi- period (u_0=0.35 m/s; Y_{A0}=0.001;T_{S0}=400°C,t_{sc}=360 s)

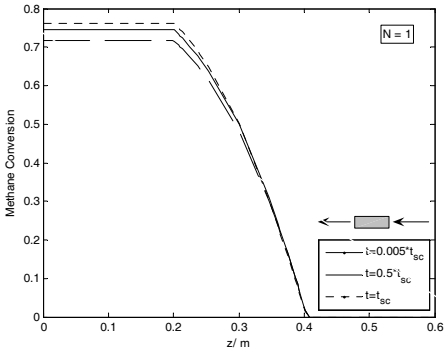

Fig.5. Evolution of methane conversion at different moments of time in the RFR, during the second semi- period (u_0=0.35 m/s; Y_{A0}=0.001; T_{S0}=400°C, t_{sc}=360 s)

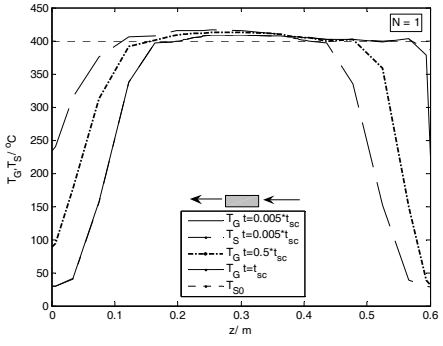

Fig.6. Evolutions of gas phase and solid phase temperatures in the RFR at different moments of time , during the second semi- period (u_0=0.35 m/s; Y_{A0}=0.001; T_{S0}=400°C, t_{sc}=360 s)

The temperature evolutions during the first two semi-periods, corresponding to an initial uniform solid bed temperature of 400°C are given in figures 4 and 6. As observed, a gas preheating zone is appearing on the first zone of inert contacted by the gas. This zone is extending in time toward the centre of the bed achieving about 15% of the bed at the end of semi-period. The heat released by combustion is continuously accumulated in the centre of the bed, where the solid temperature is increasing, the pseudo-steady state maximum temperature being about 500°C. This phenomenon is inducing an increase of the methane conversion in the bed from 70% at the start of operation to unity at the pseudo-steady state regime (Fig. 3, 5 and 7).

Fig. 7 and 8 present the evolutions of methane conversion and temperature in each phase at different moments of time, after 100 periods. As seen, the difference between the solid and gas temperatures is negligible all along the solid bed (the solid and gas temperature curves are overlapping). The temperature in the catalyst bed after reaching pseudo steady state is around 500°C and gas temperature at reactor exit varies on the interval 25-110°C.

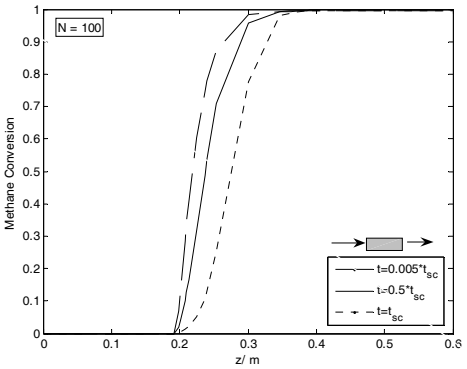

Fig.7. Pseudo steady state evolutions of methane conversion at different moments of time in the RFR, direct flow (u_0=0.35 m/s; Y_{A0}=0.001; T_{S0}=400°C, t_{sc}=360 s)

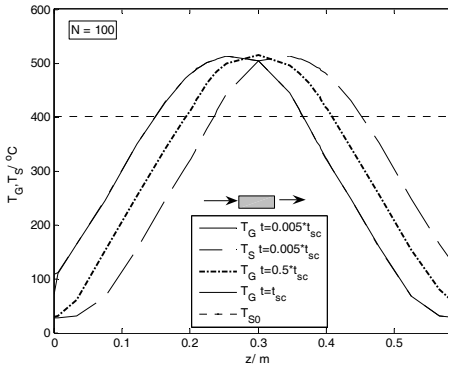

Fig.8. Pseudo steady state evolutions of gas phase and solid phase temperatures in the RFR at different moments of time (u_0=0.35 m/s; Y_{A0}=0.001; T_{S0}=400°C, t_{sc}=360 s)

From Fig. 9 and 10 we can deduce that an increase of t_{sc} from 360 to 420 s caused the bed cooling due to the increase of the heat quantity removed with the flowing gas (the cooled zone of the bed is larger and the temperature in the bed is lower, which corresponds to lower methane conversions).

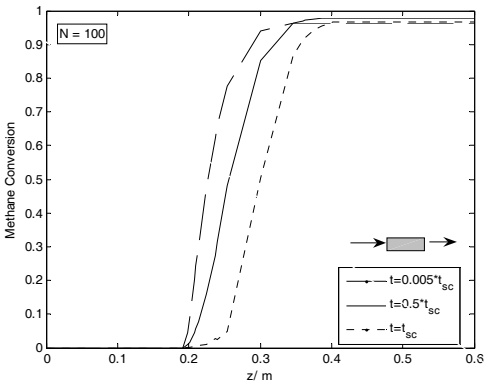

Fig.9. Pseudo steady state evolutions of methane conversion at different moments of time in the RFR, direct flow (u_0=0.35 m/s; Y_{A0}=0.001; T_{S0}=400°C, t_{sc}=420 s)

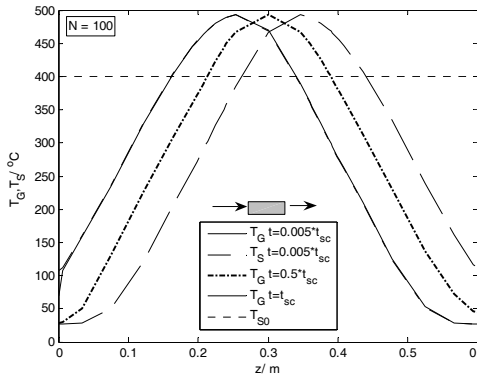

Fig.10. Pseudo steady state evolutions of gas phase and solid phase temperatures in the RFR at different moments of time (u_0=0.35 m/s; Y_{A0}=0.001; T_{S0}=400°C, t_{sc}=420 s)

As observed from Fig. 11 and 12, in order to attain the same productivity on the weight unity of catalyst, the steady state monolith reactor needs a much higher feeding temperature.

Fig. 11 and 12 evidenced also the increase of gas temperature needed to obtain total methane conversion, with gas velocity increase. Thus the monolith reactor can be operated at higher capacities (higher gas velocities) only with supplementary expenses induced by an increase of energy consumption.

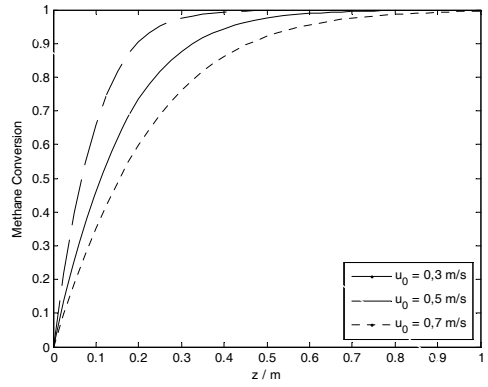

Fig.11. Evolution on methane conversion in the monolith reactor (Y_{A0} = 0.001; T_{G0} = 520°C)

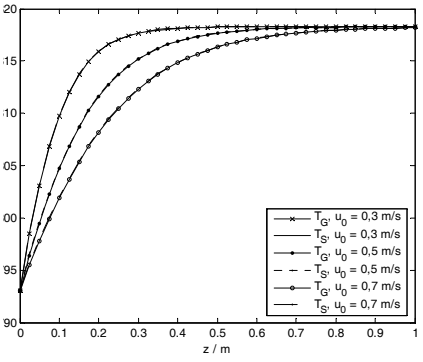

Fig. 12. Evolutions of gas phase and solid phase temperatures in the monolith reactor (Y_{A0} = 0.001; T_{G0} = 520°C)

Regarding the internal diffusion limitations, Fig. 13 and 14 present the evolutions of internal effectiveness factor for the two catalytic beds. Due to the higher temperature in the monolith reactor and relatively low grain size

considered for the packed bed calculation, the values of effectiveness factor are practically identical, with a slightly lower value for the monolith reactor.

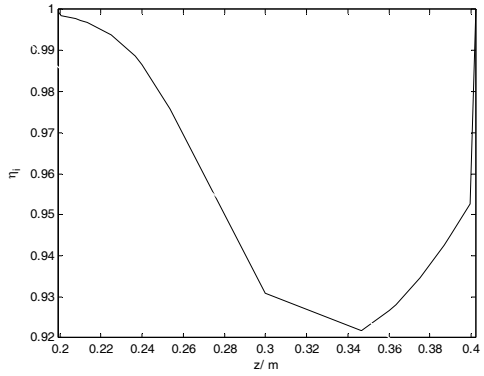

Fig. 13. Evolution of internal effectiveness factor for one semi-period in the RFR at pseudo steady state (u_0 = 0.35 m/s; Y_{A0} = 0.001; T_{S0} = 400°C, t_{sc} = 360 s)

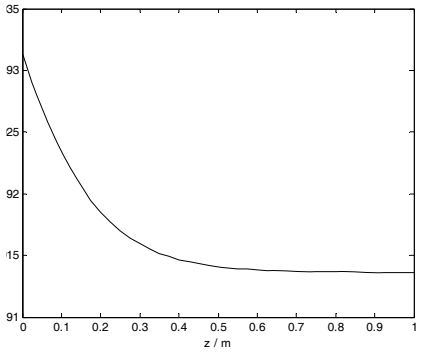

Fig. 14. Evolution of internal effectiveness factor for the monolith reactor (u_0 = 0.5 m/s; Y_{A0} = 0.001; T_{G0} = 520°C)

The temperature increase in the bed is practically equal to the maximum adiabatic temperature change, directly proportional to the feed hydrocarbon concentration. The need of gas preheating and the important quantities of heat convected out of this reactor, by the gas phase, impose the necessity of additional heat recovery equipments in order to approach autothermal regime. Of course, one of technical solutions usable could be the reverse flow operation of the monolith bed. Studies in this domain were published by Marin et al. [11]. However this presents the inconvenient of a significant lower thermal capacity of the monolith (almost two times in our case) and consequently, lower operation stability (lower semi-cycle duration). Also, another inconvenient concerns the higher cost of the monolith structures. To alleviate this limitation further investigations are necessary, by combining the advantages of monolith structures concerning the mass transfer and the effectiveness of the catalyst, with those of higher thermal heat capacity of packed bed.

4. Conclusions

Under equivalent conditions, a reverse flow operated packed bed reactor presents, comparing with a steady state monolith reactor, the advantage of a cheap and stable autothermal operation and a lower investment cost, but in conditions of a higher operating cost due to a higher pressure drop of the gas. Nevertheless, the monolithic structure offers a very convenient way to contact a solid catalyst with a flowing reactant, due to its lower pressure drop and relatively good mass-transfer characteristics. An important inconvenient of the steady state operation of this reactor, for combustion of lean methane mixtures at total methane conversion, is a

rather high feed temperature and consequently, the need of a facility for heat recovery from the effluent gas. The application of the flow reversal operation technique to this reactor is less advantageous due to its low heat storing capacity. Combinations between packed bed of coarse inert particles and monolith catalyst structures are expected to be an appropriate compromise between the shortcomings of the two reactors, providing a low pressure drop and good effectiveness of catalyst bed.

Glossary

a_v - specific gas-solid surface area, m^2_{GS}/m^3_{bed}
$c_{p,G}$, $c_{p,S}$ – specific heat capacity of gas and solid respectively, J/(kg·K)
C – total molar concentration, kmol/m^3
d_h – hydraulic diameter, m
d_p – catalyst particle diameter, m
D_A – methane molecular diffusion coefficient, m^2/s
D_e – effective diffusion coefficient of methane in the spherical catalyst particle, m^2/s
D_L – axial dispersion coefficient in a packed bed (related to interstitial gas velocity, u_i), m^2/s
Da – Damköhler number
E_a – activation energy, J/mol
ΔH_{RA} – reaction enthalpy, J/kmol
k_G - gas-solid mass transfer coefficient, m/s
k_m - apparent reaction rate constant, kmol $kg^{-1}s^{-1}$ bar^{-1}
k_s – constant rate of catalytic reaction, m/s
k_v – constant rate of catalytic reaction, s^{-1}
L – packed bed, respectively monolith channel length, m
L_C –thickness of the washcoat, m
$\overline{M}$ – average molar mass of a mixture, kg/kmol
N – number of cycles
p – gas pressure, units vary
R - universal gas constants; 0.082 m^3 bar $kmol^{-1}K^{-1}$
t – time, s
t_{sc} - cycle duration, s
T_G, T_S – gas phase respectively, solid phase temperature, K
u - superficial gas velocity, m/s
u_i - interstitial gas velocity, m/s
Y_{AG}, Y_{AS} – mole fraction of methane in the flowing gas and at the external catalyst surface respectively
z – axial coordinate, m
α – gas to solid heat transfer coefficient, W/(m^2·K)
δ_w – wall thickness of the reactor, m
ε – packed bed respectively monolith porosity
ε_g – catalyst particle porosity, $\varepsilon_g = 0.5\ m^3_{gas}/m^3_{particle}$
η_i – internal effectiveness factor, dimensionless
λ_G – gas thermal conductivity, W/(m K)
$\lambda_{L,S}$ - heat axial dispersion coefficient in the gas phase, W/(m·K)
λ_S – axial solid thermal conductivity in the packed bed, W/(m·K)
μ_G –dynamic gas viscosity, kg/(m s)

ρ_G - gas density, kg/m^3
ρ_S – density of catalyst particle, kg/m^3
Indices
0 – feeding conditions
i – initial conditions

R E F E R E N C E S

[1] *Y. Matros, A. Noskov,* Chem. Engng. Proc., **vol. 32**, 1993, pp.89-98.
[2] *Y. Matros*, Stud. Surf. Sci. Catal. – Catalytic Processes Under Unsteady-State Conditions, **vol. 43**, Elsevier, 1989.
[3] *R.E. Hayes, S.T. Kolaczkowski*, Introduction to Catalytic Combustion, Gordon and Breach Science Publishers, 1997.
[4] *Z.R. Ismagilov, M.A. Kerzhentsev*, Catal. Rev.-Sci. Eng., **vol. 32(1&2)**, 1990, pp. 51-103.
[5] *M. Zwinkels, S. Jaras, G. Menon*, Catal.Rev.-Sci.Eng., **vol. 35(3)**, 1993, pp.319-358.
[6] *A. Cybulski, J. Moulijn*, Catal. Rev. –Sci. Eng., **vol. 36(2)**, 1994, pp.179-270.
[7] *A. Cybulski, J. Moulijn*, Structured Catalysts and Reactors, CRC Press - Taylor & Francis, Boca Raton, 2006.
[8] *A. Barresi, M. Cittadini, A. Zucca*, Appl. Catal. B, **vol. 43**, 2003, pp. 27-42.
[9] *R.M. Heck, S. Gulati, R.J. Farrauto*, Chem. Engng. Journal, **vol. 82**, 2001, pp. 149-156.
[10] *M. Boşomoiu, G. Bozga, D. Berger, C. Matei*, Appl. Catal. B, doi:10.1016/j.apcatb.2008.06. 008.
[11] *P. Marin, M. Hevia, S. Ordonez, F. Diez*, Catal. Today, **vol. 105**, 2005, pp. 701-708.
[12] *C.L. Yaws*, Chemical Properties Handbook, Mc Graw Hill, 1999.
[13] *Y. Matros, G. Bunimovich*, Catal.Rev.-Sci.Eng., **vol. 38(1)**, 1996, pp. 1-68.
[14] *N. Wakao, T. Funazkri*, Chem. Eng. Sci., **vol. 33**, 1978, pp. 1375-1384.
[15] *E.U. Schlunder*, Chem. React. Eng. Rev., ACS Symp. Series, Houston, **vol. 72**, 1978, pp. 110.
[16] *H. Martin*, Chem. Eng. Sci., **vol. 33**, 1978, pp. 913-919.
[17] *N. Wakao, S. Kaguei*, Heat and Mass Transfer in Packed Beds, Gordon and Breach Science Publisher, 1982.
[18] *J. Votruba, V. Hlavacek, M. Marek*, Chem. Eng. Sci., **vol. 27**, 1972, pp. 1845-1851.
[19] *G. F.Froment, K. Bischoff*, Chemical Reactor Analysis and Design, John Wiley, N.Y., 1979.
[20] *D. Leung, R.E. Hayes, S.T. Kolaczkowski*, Can. J. Chem. Eng., **vol. 74**, 1996, pp. 94-103.
[21] *B.A. Finlayson*, Nonlinear Analysis in Chemical Engineering, Mc Graw Hill, N.Y., 1980.
[22] *J. Villermaux, D. Schweich*, Ind. Eng. Chem. Res., **vol. 33**, 1994, pp. 3025-3030.